Chapter 9

Applications of CVD to Produce Thin Films for Solid-State Devices

A.M. Torres-Huerta, M.A. Domínguez-Crespo and
A.B. López-Oyama

Additional information is available at the end of the chapter

http://dx.doi.org/10.5772/63964

Abstract

Thin films of Pt-YSZ and Pd-ZrO_2 cermets by chemical vapor deposition (CVD) from metallorganic precursors (MOCVD) were evaluated as electrode in solid-state devices. Morphology and structural characteristics were studied by X-ray diffraction (XRD), scanning electronic microscopy, atomic force microscopy (AFM), and transmission electronic microscopy (TEM). Electrochemical performance was determined using Tafel and electrochemical impedance spectroscopy methods. Metallorganic precursors were used (metal-acetylacetonates), and argon and oxygen were used as the carrier and reactive gases, respectively. The particle average size was less than 20 nm, with high and uniform particle dispersion according to TEM measurements.

Keywords: thin films, CVD, platinum metals, zirconia, cermets

1. Introduction

Chemical vapor deposition (CVD) is a fast and economic method to obtain controlled deposits of high quality; the main drawbacks are the possible incorporation of impurities due to non-exhausted remains and poor adhesion of the film in some cases [1]. Chemical vapor deposition (CVD) from metallorganic precursors (MOCVD) is a rapidly developing method for producing films and coatings of ceramic materials for a variety of applications [2]. Among solid electrolyte cells, commonly used for numerous applications including gas sensors, gas pumps, solid oxide fuel cells, and electrochemically promoted catalysts, platinum electrode deposited on yttria-stabilized zirconia (YSZ) is one of the most widely studied examples [3] because of

YSZ conducts at temperatures above 300°C via O^{2-} diffusion and platinum has always been of particular interest due to its electrocatalytic properties [4]. The electrochemical performance of electrode layers depends largely on the microstructure of the three-phase boundaries (TPBs) [5] in which the ionic conductor, the electronic conductor, and the oxygen gas are in contact, being the best pathway to reduce oxygen to oxygen ion at the surface [6].

Nanoparticles exhibit very interesting features at the nanometer scale due to the quantum confinement, where the changes induced to the microstructure allow them to increase the specific surface area and, in the case of electrodes, more TPBs are arisen. These characteristics are desirable for high electrochemical performance. The higher sintering temperatures are related to the formation of undesirable reaction products highly resistive at the electro/electrolyte interface. By reaching the nanometer size, the sintering temperature can be low facilitating the ceramic processing, due to the more TPBs which as a geometrical parameter required for high electrochemical performance [5].

The appearance of the material at nanometric scale can be achieved by modification of the preparation methods despite its identical chemical composition. The material undergoes a phase transformation by changing temperature and pressure or by combining different materials. The induced changes onto the microstructure modify the electrode behavior [4]. One approach to increase the TPBs areas, and in consequence the yield of the electrodes, is to prepare a cermet material that spreads the solid electrolyte into the electrode [5, 7–10]. The development in thin-film technology and the application of ionic-electronic composites as electrodes have significantly reduced the ohmic loss caused by the electrolyte [5]. The rate and selectivity of catalytic reactions occurring on metal and metal-oxide porous catalyst-electrode films deposited on solid electrolytes can be reversibly affected in a very pronounced and controlled manner by polarizing of the catalyst-electrode, which can exceed the corresponding rate of ion transport through the solid electrolyte by several orders of magnitude [11]. Noble metals are historically known to be extremely non-reactive, but the possibility for obtaining coatings of platinum metals by means of CVD on the substrates made of different materials was demonstrated widely [12]. Metal, oxide, and metal-oxide composite systems can be obtained by means of CVD using the process of thermal decomposition of a mixture of the volatile initial metal complexes with organic ligands (precursors) on a heated surface [12]. Additionally, chemical vapor deposition (CVD) is one of the most important synthesis processes for making nanoparticles of metals, semiconductors, and magnetic materials. In some cases, Pt is deposited as continuous films whereas in other cases, it is preferred in the form of a dispersion of particles with a high surface area. On the other hand, ceramics based on zirconium dioxide (zirconia, ZrO_2) are promising materials for multifunctional applications. In previous works [13–16], ZrO_2, IrO_2, Pt, and IrO_2-YSZ thin films have been synthesized by MOCVD process and, in the case of ZrO_2, a thermodynamic study to explain the phase and the conditions that promote the formation of pure ZrO_2 from a β-diketonate precursor (Zr-acetylacetonate, $Zr(acac)_4$) and oxygen (O_2) as carrier/reactive gas was reported [17], and now, the structural, nanocrystalline nature and morphological characterizations of Pt-YSZ composites are completed and reported; furthermore, in order to determine the performance of these composites as electrodes in YSZ solid-state devices, electrochemical tests were also carried out.

http://dx.doi.org/10.5772/63964

Additionally, the synthesis of Pd-ZrO_2 cermets by MOCVD and their characterization are reported. X-ray diffraction (XRD), atomic force microscopy (AFM), scanning electron microscopy (SEM), Raman spectroscopy, and electrochemical characterizations were conducted in order to determine the structure, composition, morphology, oxidation state, and electrocatalytic properties of these materials. Metallorganic precursors were used (metal-acetylacetonates), and argon and oxygen were used as the carrier and reactive gases, respectively.

2. Experimental procedure

The experimental setup has been described elsewhere [15]. Amorphous quartz and YSZ were used as substrates; the composite electrodes were produced by a horizontal hot wall MOCVD. The employed precursors were $Zr(acac)_4$, $Y(acac)_3$, $Pt(acac)_2$, and $Pd(acac)_2$ [Sigma-Aldrich, ≥97%]. Argon and oxygen gases were used as the carrier and reactive gases, respectively. Before the MOCVD process, the quartz substrates were cleaned with a soapy solution and thereafter rinsed with tap water, deionized water, and acetone. The optimal experimental conditions for producing nanocomposite electrodes were identified as follows: 450–600°C deposition temperature (T_{dep}), 1.0 Torr total pressure (P_{tot}), 190–220°C precursor temperature (T_{prec}), 130 sccm O_2, and 180 sccm Ar flow rates (FR). The structural analysis and the particle size determination were carried out by X-ray diffraction (XRD, Siemens D5000 and Bruker D8 Advanced) using a monochromatic Cu-$K_{\alpha 1}$ radiation at 35 kV, 25 mA and a scan rate of 0.02° min^{-1}; the average crystallite size was calculated from the diffraction peak broadening using the Scherrer equation; and the morphology, texture, and surface roughness of the films were examined by scanning electron microscopy (SEM, JEOL JSM-6300), transmission electron microscopy (TEM, JEOL-2000 FX-II), and atomic force microscopy by AFM, Nanosurf easyscan 2 AFM/STM in contact mode with a Si cantilever and nominal force of 20 nN, respectively.

Finally, the electrochemical tests were conducted to determine the performance of these films as electrodes. The method for this purpose was a three terminal one: the working electrode (WE, 1.7 cm^2 in area) on one side of the YSZ pellet and the reference and the counter electrodes on the opposite side (RE, 0.5 cm^2 in area, CE, 1.2 cm^2 in area, respectively). Impedance measurements were carried out over the frequency range of 10^5–10^{-2} Hz using a Solartron 1255 frequency response analyzer from 300 to 800°C in air. The signal applied to the cell was generally 10 mV rms. Potentiodynamic polarization was obtained from -400 mV to +400 mV at a scan rate of 1.67 mV s^{-1}.

3. Results and discussion

Figure 1a and **b** shows XRD spectra of platinum thin films obtained at 500°C and 550°C, and quartz is shown as reference (**Figure 1c**). Pt crystallites in face-centered cubic structure (ICDD 04-0802) grow in (1 1 1) orientation at 500°C while at 550°C, is polycrystalline, and at both temperature, the films are purely metallic and shiny. The broadening of the reflections was associated with a small crystallite size, determined by Scherrer equation:

$$t = \frac{0.9\lambda}{B\cos\theta_B} \tag{1}$$

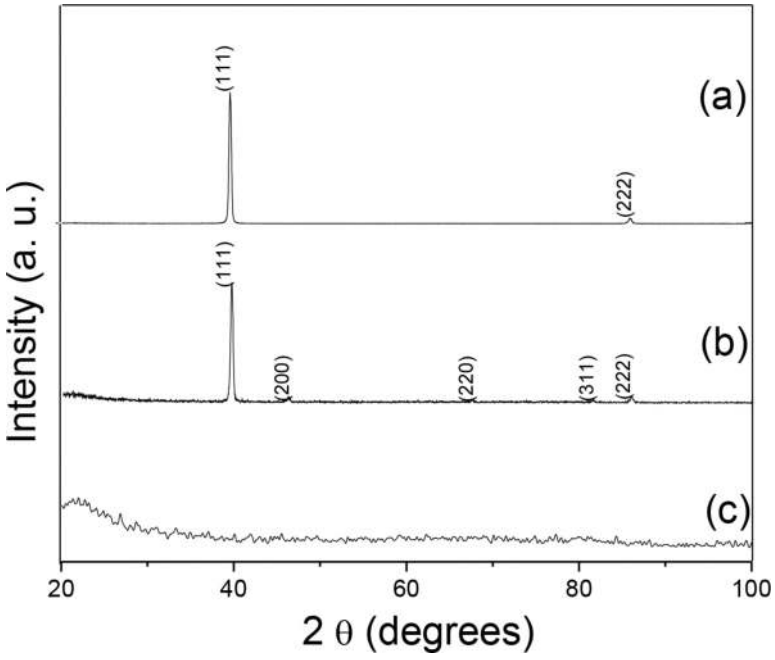

Figure 1. Pt thin-film diffractograms (a) 500°C, (b) 550°C and (c) amorphous quartz.

Here, t is the mean crystalline size, λ is the wavelength of the X-ray, B is the full width of a peak at half of the maximum of the peak (FWHM) in the diffraction spectra (measured in radians), and θ is the Bragg angle.

Then, the mean Pt crystallite size was 48 nm. Pt-ZrO_2 composite was obtained at 600°C (**Figure 2a**); ZrO_2 signals are weak, while Pt reflections are better defined than that for ZrO_2. It was reported before that ZrO_2 at these particular experimental conditions was not obtained below 600°C [16]; the Pt-ZrO_2 composites had to be synthesized at this temperature, taking in account the experimental conditions for ZrO_2, that is, only oxygen was used as the carrier and reactive gas. The next step was the deposition of yttria-stabilized zirconia (YSZ), shown in **Figure 3b**. These films were transparent. The XRD spectrum displays the signals corresponding to (1 1 1), (2 0 0), and (3 1 1) planes for cubic YSZ (ICDD 30-1468); the Zr/Y weight ratio to obtain YSZ was 0.87:0.13, according to Wang et al. [18]; the mean crystallite size was 15 nm. The appearance of YSZ cubic microstructure could be the result of these nanocrystalline sizes [19, 20]. The formation of cubic structure of YSZ film at low temperatures is somewhat alike with the formation of metastable tetragonal structure as a result of nanocrystalline size effect in the transformation of zirconium phase [18, 19, 21]. Finally, once the individual thin films

http://dx.doi.org/10.5772/63964

were synthesized, the composite Pt-YSZ was deposited by combining the different experimental conditions (**Figure 3c**). The signals of both Pt and YSZ are clearly observed. In this case, the mean Pt crystallite size was 21 nm, while the YSZ size remains the same, 15 nm. The decrement in Pt crystallite size could be attributable to the film microstructure, which is avoiding the agglomeration, sintering, and, consequently, the growth of Pt particles. The XRD spectrum for amorphous quartz is shown in **Figures 1c**, **2b**, and **3a** in order to identify the signals arising from thin films. Experimental deposition conditions are summarized in **Table 1**.

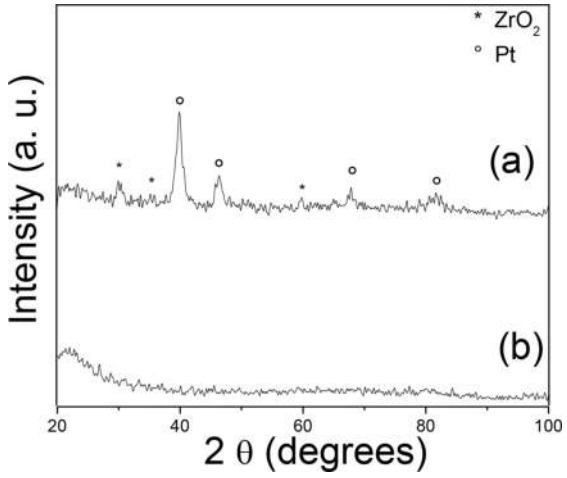

Figure 2. Pt-ZrO_2 diffractograms (a) 600°C and (b) amorphous quartz.

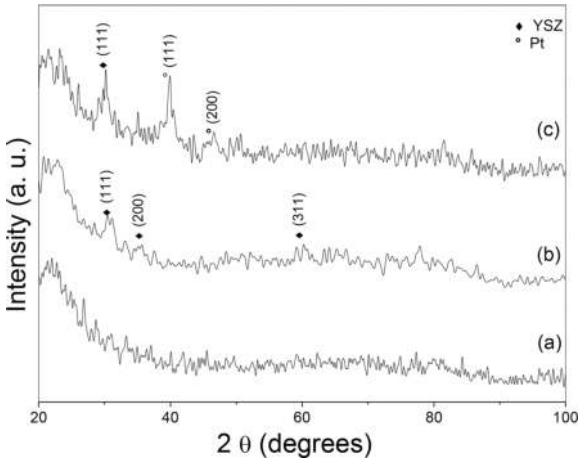

Figure 3. Diffractograms of (a) amorphous quartz, (b) YSZ, and (c) Pt-YSZ at 600°C.

Thin film	T_{prec} (°C)	T_{dep} (°C)	Gas flow (cm³/min)
Pt	180	500	180
ZrO_2	220	600	130
Pt-ZrO_2	220	550	130
Y_2O_3-ZrO_2	220	600	130
Pt-YSZ	220	600	130

Table 1. Experimental deposition conditions for Pt-YSZ film.

A typical view of the composite Pt-YSZ film is given in **Figure 4**. The film is porous as a result of its columnar growth (**Figure 4d**, cross-sectional view). Thickness of the film was estimated to be about 1 μm with a growth rate of 50 nm/min.

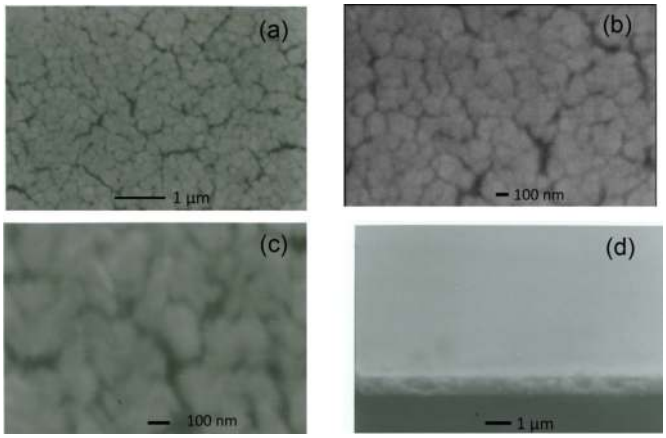

Figure 4. SEM images of Pt-YSZ thin films (a–c) surface and (d) cross-section.

Figure 5 depicts the impedance spectrum at 300–800°C for Pt-YSZ nanocomposite electrode films prepared on YSZ pellets. According to the associated capacitance value (10^{-5} F), reactions of charge transfer at the electrode/electrolyte interface were assigned to the small semicircle at high frequency. It seems that a diffusion mechanism rise at the low-frequency region because of the large semicircle with capacitance values between 10^{-4} and 10^{-3} F, attributed to the oxygen diffusion at the finite thickness in the film. The bulk and grain boundary responses are missing due to the frequency scale. According to West et al. [22], $C = \sim 10^{-7}$ F corresponds to electrode-electrolyte interphase and $C = \sim 10^{-4}$ F is associated with the oxygen electrochemical reaction into the TPB; furthermore, a depressed semicircle could indicate an associated impedance to the oxygen path through the electrode [22]. The Pt-YSZ nanocomposite electrodes displayed lower charge-transfer resistance than diffusion resistance even at higher temperatures. This suggests easy interfacial charge-transfer reactions probably controlled by the diffusion of oxygen through the structure of the Pt-YSZ electrode.

http://dx.doi.org/10.5772/63964

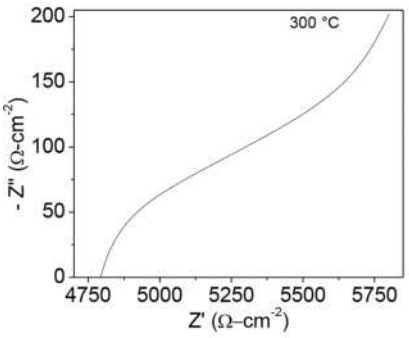

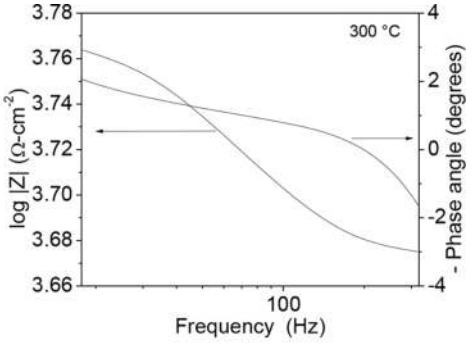

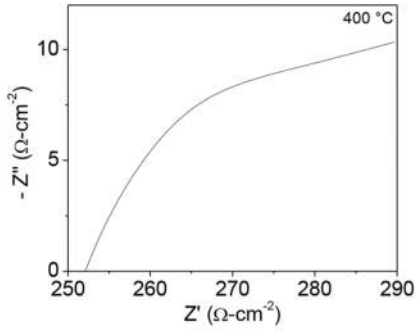

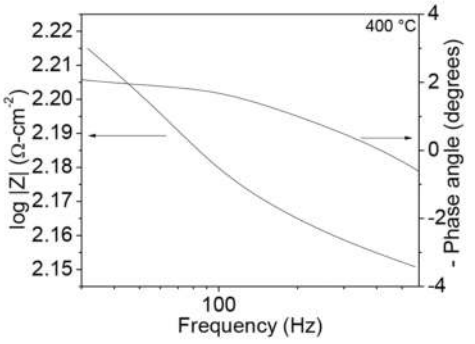

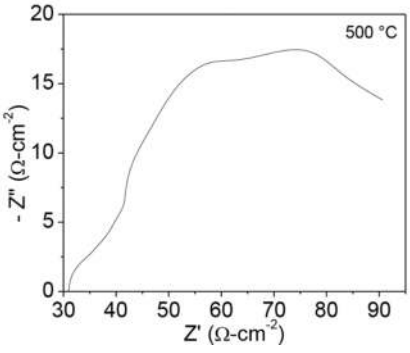

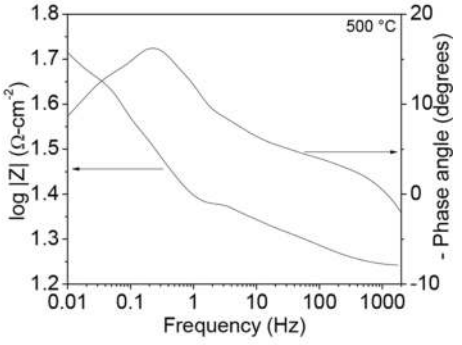

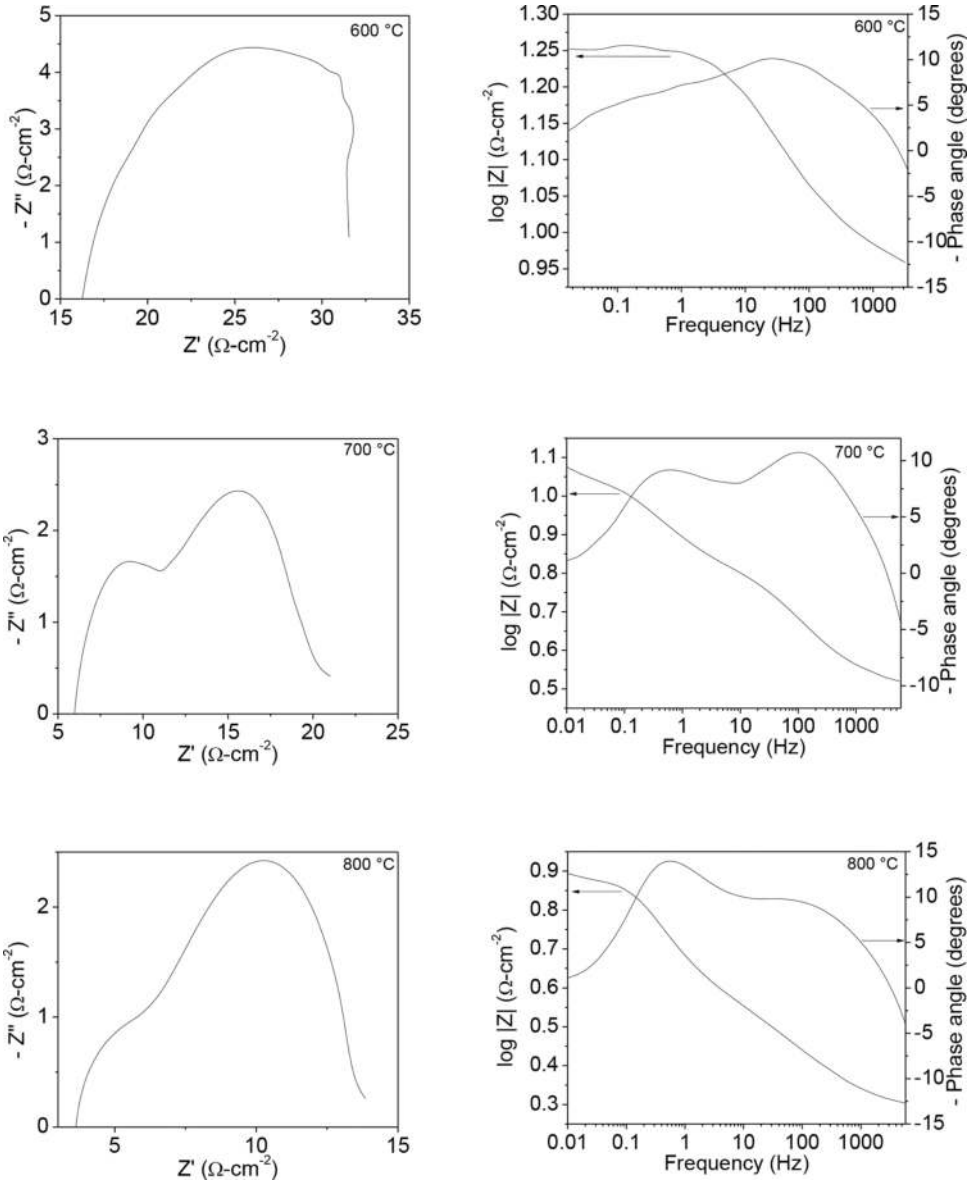

Figure 5. Impedance spectrum at 300–800°C for Pt-YSZ nanocomposite electrode films prepared on YSZ pellets.

From polarization plots (Tafel plots) can be observed that as temperature increases, the current increases through the electrode-electrolyte interphase (**Figure 6**). In the anodic branch where higher current was obtained than that obtained in cathodic branch, except at 600 and 700°C, at 600°C, the current in the cathodic branch is slightly higher than in anodic branch; and at

http://dx.doi.org/10.5772/63964

700°C, both values of currents (anodic and cathodic branches) seem to be the same; and the cathodic response looks similar at these temperatures (600 and 700°C). At 800°C, the cathodic response is lower than that observed at 600 and 700°C, but the current increases as temperature increases in the anodic branch. This behavior could be attributed to a decrement of TPB provoked by particle agglomeration, maybe Pt or YSZ, or by a reaction between Pt and YSZ as Badwal and de Bruin suggested [23]. **Table 2** shows the interchange current and Tafel slopes from **Figure 6**. According to the Tafel slopes, one order of reaction was obtained. Besides YSZ, no oxidized phases were found in Pt-YSZ electrodes after heating in air, which indicates a high thermal stability (**Figure 7**).

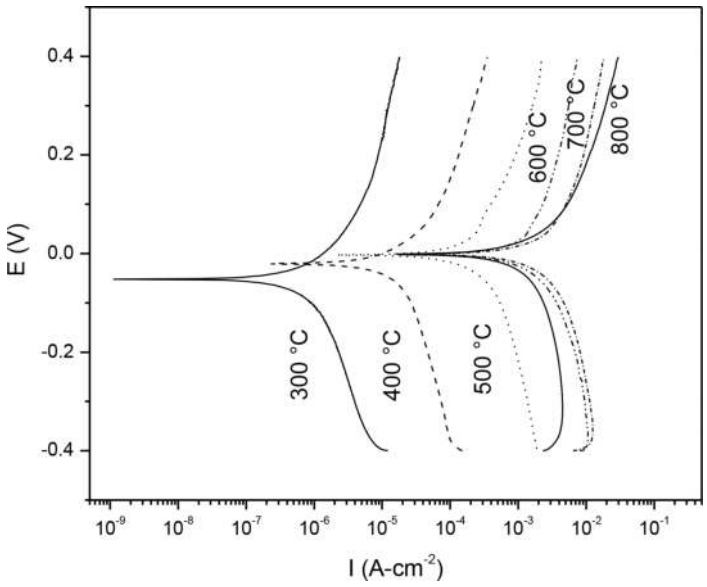

Figure 6. Tafel plots of Pt-YSZ at 300–800°C.

Temperature (°C)	Log I_o	Cathodic part	Anodic part
	(A/cm²)	m_c (mV/decade)	m_a (mV/decade)
300	-6.22	-242	190
400	-4.76	-204	214
500	-3.62	-173	254
600	-2.77	-177	165
700	-2.43	-167	177
800	-2.67	-122	211

Table 2. Interchange current (I_o) and Tafel slopes (m), from Pt-YSZ.

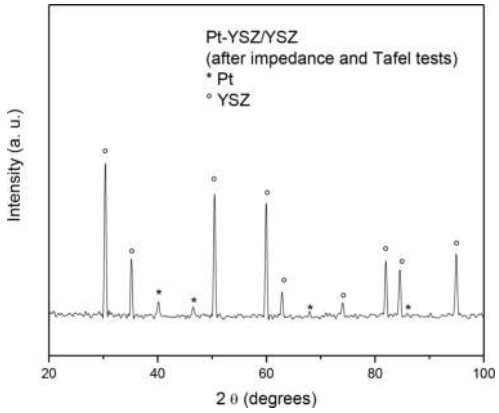

Figure 7. XRD pattern of Pt-YSZ/YSZ after impedance and Tafel tests.

The synthesis of cermets Pd-ZrO_2 by MOCVD and their characterization were conducted in order to determine the structure, composition, morphology, oxidation state, and electrocatalytic properties of these materials. Metallorganic precursors were used (metal-acetylacetonates), and argon and oxygen were used as the carrier and reactive gases, respectively. It is expected that these materials could be applied in water purification. The composite thin films were prepared using a ratio of Pd and Zr metals of 10–90 wt%, respectively. The deposition temperature (T_{dep}) was varied from 450, 500, and 550°C, and pressure (P) was controlled at 1.0 Torr. According to XRD patterns (**Figure 8**), palladium metallic reflections are difficult to observe and only in the films at 500°C, these signals are detected. Pd-ZrO_2 coatings on stainless

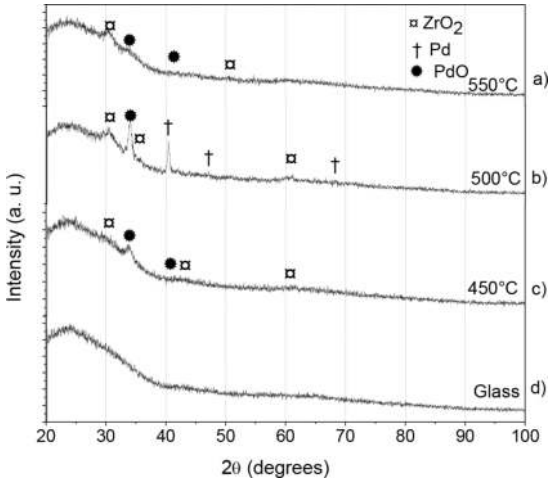

Figure 8. XRD patterns of Pd-ZrO_2 on glass substrate deposited at (a) 450°C, (b) 500°C, and (c) 550°C for 30 min and 80–20% volume Ar-O_2 and (d) of glass.

http://dx.doi.org/10.5772/63964

steel were deposited to characterizing their electrochemical behavior. It was reported that an increasing in Pd concentration favors the zirconia tetragonal phase as well as a higher crystal size [24]. The Pd-ZrO_2 coatings deposited on glass substrates were porous, uniform and thin (**Figure 9**). Apparently, the films exhibit good adherence, but an adherence test is needed to verify this appreciation; composites obtained at 450°C show higher porosity. **Figure 10** shows the AFM images for Pd-ZrO_2 at different temperatures; it can be suggested a columnar growth, characteristic for this type of technique and thin film. The average roughness is present in **Table 3**. Pd-ZrO_2 coatings on stainless steel, at 450 and 500°C, were uniform, and it is observed at the domes, which could indicate a columnar growth (**Figure 11**). The coatings display a shift in the corrosion potential (**Figure 12**) from 64 mV to 273 mV as consequence of deposition temperature.

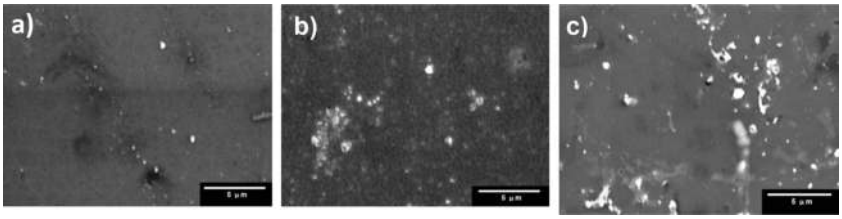

Figure 9. Scanning electron micrographs of Pd-ZrO_2 on glass substrate deposited at (a) 450°C, (b) 500°C, and (c) 550°C for 30 min and 80–20% volume Ar-O_2.

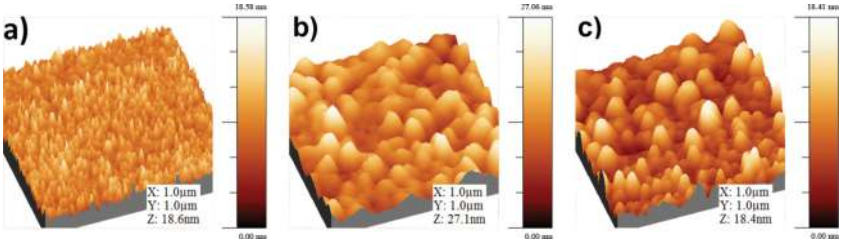

Figure 10. AFM micrographs of Pd-ZrO_2 on glass substrate deposited at (a) 450°C, (b) 500°C, and (c) 550°C for 30 min and 80–20% volume Ar-O_2.

Temperature (°C)	Rms (nm)
AISI 304L	6.1
450	6.3
500	15.9
550	3.7

Table 3. Average roughness for Pd-ZrO_2 thin films.

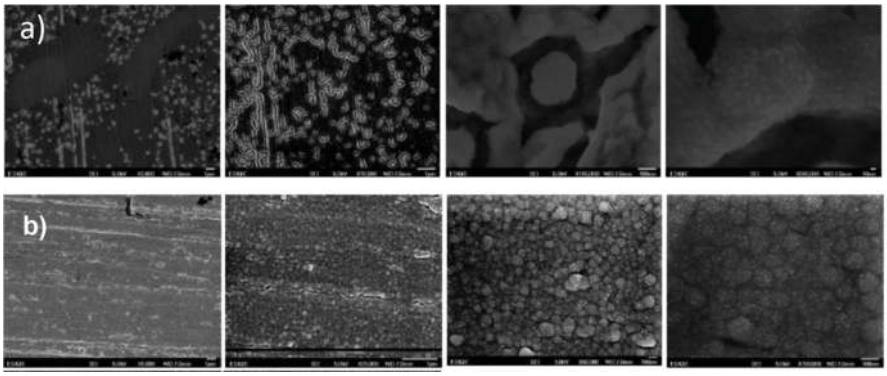

Figure 11. SEM micrographs of Pd-ZrO_2 on stainless steel at (a) 450°C and (b) 500°C.

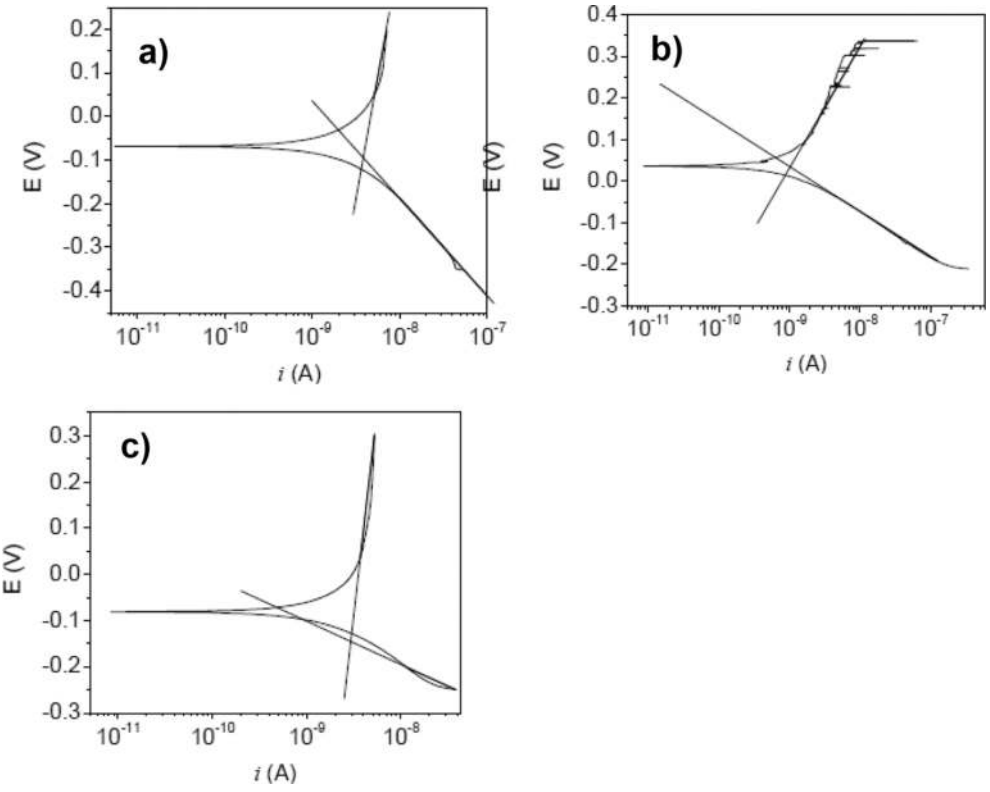

Figure 12. Tafel plot for Pd-ZrO_2 coatings on stainless steel at (a) 450°C, (b) 500°C, and (c) 550°C.

http://dx.doi.org/10.5772/63964

4. Conclusions

Metal, oxide, and metal-oxide composite systems can be obtained by means of CVD using the process of thermal decomposition of a mixture of the volatile initial metal complexes with organic ligands (precursors) on a heated surface. The possibility for obtaining coatings of platinum metals by means of CVD on the substrates made of different materials was demonstrated widely. The platinum-YSZ particle average size was less than 20 nm, with high and uniform particle dispersion according to TEM measurements.

Acknowledgements

Authors are grateful for the financial support by CONACYT, SNI, and IPN in the projects SIP2016-0541, and they thank J. Ferretiz-Anguiano, J.R. Vargas-García, and H. Dorantes for their technical support.

Author details

A.M. Torres-Huerta[1*], M.A. Domínguez-Crespo[1] and A.B. López-Oyama[1,2]

*Address all correspondence to: atohuer@hotmail.com and atorresh@ipn.mx

1 National Polytechnic Institute, CICATA-Altamira, Altamira, Tamaulipas, Mexico

2 CONACYT, Cd. México, Mexico

References

[1] C. Thurier, P. Doppelt. Coordination Chemistry Reviews 252 (2008) 155–169.

[2] S.P. Krumdieck, O. Sbaizero, A. Bullert, R. Raj. Surface and Coatings Technology 167 (2003) 226–233.

[3] G. Fóti, A. Jaccoud, C. Falgairette, C. Comninellis. Journal of Electroceramics 23 (2009) 175–179.

[4] A. Jaccoud, G. Fóti, R. Wüthrich, H. Jotterand, Ch. Comninellis. Topics in Catalysis 44 (2007) 409–417.

[5] A.J. Darbandi, T. Enz, H. Hahn. Solid State Ionics 180 (2009) 424–430.

[6] C. Lee, J. Bae. Solid State Ionics 179 (2008) 2031–2036.

[7] K. Sasaki, J.P. Wurth, R. Gschwen, K. Godickemeier, L.J. Gauckler. Journal of the Electrochemical Society 143(2) (1996) 530.

[8] T. Tsai, S.A. Barnett. Solid State Ionics 93 (1997) 207.

[9] T. Kenjo, M. Nishiya. Solid State Ionics 57 (1992) 295.

[10] M.J.L. Ostergard, C. Clausen, C. Bagger, M. Mogensen. Electrochimica Acta 40(12) (1995) 1971.

[11] N. Kotsionopoulos, S. Bebelis. Journal of Applied Electrochemistry 35 (2005) 1253–1264.

[12] I.K. Igumenov, N.V. Gelfond, P.S. Galkin, N.B. Morozova, N.E. Fedotova, G.I. Zharkova, V.I. Shipachev, E.F. Reznikova, A.D. Ryabtsev, N.P. Kotsupalo, V.I. Titarenko, Yu.P. Dikov, V.V. Distler, M.I. Buleev. Desalination 136 (2001) 273–280.

[13] A.M. Torres-Huerta, J.R. Vargas-Garcia. Journal of Metastable Nanocrystalline Materials 20–21 (2004) 393–398.

[14] A.M. Torres-Huerta, J.R. Vargas-Garcia. Journal Metastable Nanocrystalline Materials 24–25 (2005) 399–402.

[15] A.M. Torres-Huerta, J.R. Vargas-Garcia, M.A. Dominguez-Crespo. Solid State Ionics 178 (2007) 1608–1616.

[16] A.M. Torres-Huerta, M.A. Domínguez-Crespo, E. Ramírez-Meneses, J.R. Vargas-García. Applied Surface Science 255 (2009) 4792–4795.

[17] A.M. Torres-Huerta, J.R. Vargas-Garcia, M.A. Dominguez-Crespo, J.A. Romero-Serrano. Journal of Alloys and Compounds 483 (2009) 394–398.

[18] H.B. Wang, C.R. Xia, G.Y. Meng, D.K. Peng. Materials Letters 44 (2000) 23–28.

[19] Y. Jiang, J. Gao, M. Liu, Y. Wang, G. Meng. Solid State Ionics 177 (2007) 3405–3410.

[20] H.Z. Song, H.B. Wang, S.W. Zha, D.K. Peng, G.Y. Meng. Solid State Ionics 156 (2003) 249.

[21] J.S. Lee, T. Matsubara, T. Sei, T. Tsuchiya. Journal of Materials Science 32 (1997) 5249.

[22] A.R. West, D.C. Sinclair, N. Hirose. Journal of Electroceramics 1 (1997) 65.

[23] S.P.S. Badwal, H.J. de Bruin. Physica Status Solidi A 54 (1979) 261.

[24] E.M. Holmgreen, M.M. Yung, U.S. Ozkan. Journal of Molecular Catalyst A: Chemical 270 (2007) 101–111.